Validation of Model-Based Brain Shift Correction in Neurosurgery via Intraoperative Magnetic Resonance Imaging: Preliminary Results

Ma Luo*[a], Sarah F. Frisken[b], Jared A. Weis[a], Logan W. Clements[a], Prashin Unadkat[b], Reid C. Thompson[c], Alexandra J. Golby[b], Michael I. Miga[a,c,d]

[a]Department of Biomedical Engineering, Vanderbilt University, Nashville, TN, USA 37232; [b]Department of Radiology, Brigham and Women's Hospital, Boston, MA, USA 02115; [c]Department of Neurological Surgery, Vanderbilt University Medical Center, Nashville, TN, USA 37232; [d]Department of Radiology and Radiological Sciences, Vanderbilt University Medical Center, Nashville, TN, USA 37232

ABSTRACT

The quality of brain tumor resection surgery is dependent on the spatial agreement between preoperative image and intraoperative anatomy. However, brain shift compromises the aforementioned alignment. Currently, the clinical standard to monitor brain shift is intraoperative magnetic resonance (iMR). While iMR provides better understanding of brain shift, its cost and encumbrance is a consideration for medical centers. Hence, we are developing a model-based method that can be a complementary technology to address brain shift in standard resections, with resource-intensive cases as referrals for iMR facilities. Our strategy constructs a deformation 'atlas' containing potential deformation solutions derived from a biomechanical model that account for variables such as cerebrospinal fluid drainage and mannitol effects. Volumetric deformation is estimated with an inverse approach that determines the optimal combinatory 'atlas' solution fit to best match measured surface deformation. Accordingly, preoperative image is updated based on the computed deformation field. This study is the latest development to validate our methodology with iMR. Briefly, preoperative and intraoperative MR images of 2 patients were acquired. Homologous surface points were selected on preoperative and intraoperative scans as measurement of surface deformation and used to drive the inverse problem. To assess the model accuracy, subsurface shift of targets between preoperative and intraoperative states was measured and compared to model prediction. Considering subsurface shift above 3 mm, the proposed strategy provides an average shift correction of 59% across 2 cases. While further improvements in both the model and ability to validate with iMR are desired, the results reported are encouraging.

Keywords: Brain shift, finite element modeling, image guided surgery

1. INTRODUCTION

Critical to the success of image guided neurosurgery (IGNS) is the ability to accurately locate surgical tools in the context of preoperative imaging data. The quality of brain tumor resection procedures has greatly benefited from the evolution of IGNS over the years. More specifically, IGNS technology has been leveraged by surgeons to better localize tumor regions, assess tumor margins, plan surgical approaches, and navigate the surgical field in real-time. However, soft tissue deformation during neurosurgery, also known as brain shift, can significantly jeopardize the quality of IGNS by creating a misalignment between the preoperative imaging data and the intraoperative brain anatomy of the patient. Studies have shown cortical surface deformation up to 24 mm, and subsurface deformation ranging between 3 and 7 mm during surgery is quite common [1-4].

To address brain shift, several approaches have been proposed. One method is direct intraoperative imaging, namely ultrasonography (US), computed tomography (CT), and magnetic resonance (MR). Intraoperative US and CT, though powerful, do have limitations with respect to soft tissue contrast and workflow usage; also, in the case of iCT, radiation exposure is a concern [3-6]. With respect to adopted technologies, currently the only widely adopted solution for monitoring brain shift has been iMR [6]. The impact of iMR is shown in Nimsky et al., which reports that in 55 of 200 cases (27.5%),

the usage of iMR aided in modifying surgical strategy (e.g. further resection when residual tumor was revealed on iMR) in a variety of procedures [7]. Similarly, a wider review by Maurer et al. reports that the need for iMR-enhanced brain tumor resection was found in approximately 30% of cases [8]. Both studies suggest that the cost-to-benefit ratio of iMR needs to be considered, and provide impetus for complementary technologies such as model-based approaches for brain shift.

Going further, the essence of most computational modeling approaches that have minimal encumbrance is the desire to drive such platforms with sparse intraoperative information and to use some form of biomechanical model built on preoperative patient-specific data. The exact instrumentation make-up or even the selection of constituitive model is a subject of intense interest within the literature [9]. While the research in modeling brain shift continues to evolve, one of the greatest challenges facing these approaches that is not often discussed is the difficulties associated with validation. A number of studies have employed different validation designs. A common approach is to use realistic phantoms that attempt to recreate surgical deformations such as in Reinertsen et al. and DeLorenzo et al. [10, 11]. While phantom validation study is a viable first step to simulate a more controlled environment where factors can be easily manipulated to gauge correction performance, a full validation requires the examination of model behavior within the clinical environment. Another validation approach is to compare the model prediction with postoperative MR image volumes. In Dumpuri et al., subsurface landmarks among preoperative, postoperative and model updated MR images were used as measurements of subsurface deformation—a comparison between the measured deformation and model predicted deformation provides an assessment of the model's ability to recover intraoperative brain shift [12]. Though the use of postoperative imaging data provides a better evaluation of the model-based approach in patient data, the natural recovery of brain shift over time casts some uncertainty in the conclusions drawn from such studies [1, 12].

Ideally one would want to validate the model with intraoperatively sampled data. One study by Simpson et al. attempted to swab the tumor resection cavity immediately following resection, and then register the cavity to the preoperative MR both with and without model-based correction [13]. The results demonstrated improvement in all cases, with 6 of the 8 cases having an average correction ranging from 63% to 77% [13].

Another common approach is to use iMR data as a source of comparison. A few groups have attempted to validate their model-based methods via iMR. Skrinjar et al. is an early effort to validate a model-based brain shift correction algorithm with iMR in two patient cases by identifying 14 landmarks in each case [14]. More recently, Zhang et al. used iMR to examine their linear elastic model-based method with 25 landmarks in five patients [15]. Other groups, such as Joldes et al. and Vigneron et al., have similarly used iMR to validate their model-based approach; however, they have chosen to avoid using landmarks for validation, noting potential subjective errors in landmark designations, and have used other measurements such as modified Hausdorff distance as a metric of model accuracy assessment [16, 17]. In this study, we are reporting our validation experience in two patient cases with iMR, as the latest development in the ongoing validation effort of our deformation atlas based approach.

2. METHODOLOGY

2.1 Overview

This preliminary validation study has 4 stages: (1) generation of a patient-specific finite element mesh; (2) generation of a deformation atlas; (3) deformation correction, or model prediction of volumetric deformation; (4) quantitative assessment of the model performance in recovering intraoperative brain shift. For this study, preoperative and intraoperative MR images of two patients were acquired via Siemens 3T scanners at Brigham and Women's Hospital (Boston, MA). For each patient, the approximated craniotomy size and location were provided as well. Both patients provided written consent prior to imaging for this Brigham and Women's Hospital Institutional Review Board approved study.

2.2 Mesh Generation

The brain volume and tumor volume were manually segmented from the preoperative MR image volume of the patient using ITK-Snap [18]. The segmented brain was used to extract a surface via a marching cubes algorithm followed by a surface smoothing step. A custom-built mesh generator was then used to produce a volumetric tetrahedral mesh. For the two cases considered, the average size of the mesh was approximately 80,000 linear tetrahedral elements and approximately 17,000 nodes.

Furthermore, the patient brain image volume was rigidly registered to an atlas brain volume that has been expertly segmented via an in-house implementation of normalized mutual information, followed by a non-rigid registration using the adaptive bases algorithm [19]. The rigid and non-rigid registrations were applied to critical structures segmented from the atlas brain volume, including the falx cerebri, brain stem, and tentorium cerebelli, mapping them to patient space for patient specificity. Before proceeding to atlas generation, a visual inspection is performed using Paraview to verify the locations of the brain mesh, tumor (in red), craniotomy (in blue), critical structures such as falx, tentorium, and brain stem, shown in Figure 1 [20].

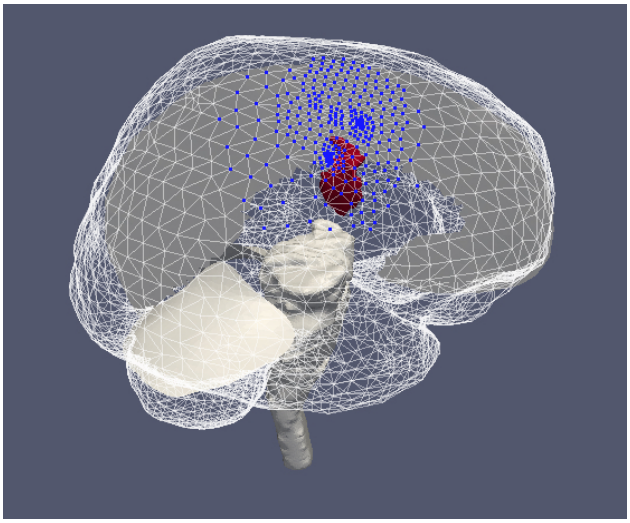

Figure 1. Mesh of a patient specific brain, with tumor (red) and craniotomy nodes (blue) included. Atlas falx, tentorium and brain stem are registered to the patient space by applying rigid and non-rigid registrations.

2.3 Atlas Generation

Following the generation of the patient-specific mesh, displacement and pressure boundary conditions were prescribed in accordance with our previous publications [1, 12, 21-23]. Briefly, for displacement boundary conditions, the brain stem area was given fixed Dirichlet conditions with no displacement; the region of the head that experiences the highest elevation, defined as above an empirically determined plane, was assigned stress free, which permits movement away from the cranial wall; the falx and tentorium were designated with slip condition, i.e. movement tangent to the dural septa is permitted, yet movement in the direction normal or through the septa is prohibited. The remaining brain surface is also modeled with a slip condition. As for pressure boundary conditions, nodes above the CSF drainage level were assumed to be constant at atmospheric pressure, while nodes below the CSF level were not permitted to allow drainage, i.e. no flux.

Our deformation atlas-based approach simulates three types of brain shift, namely gravity-induced, mannitol-induced and swelling-induced shifts. For gravity-induced shift, 3 different empirically determined CSF levels were modeled and were considered with and without the tumor in the mesh, yielding 6 potential configurations at a given head orientation. For mannitol-induced shift, 3 different empirically determined permeability conditions were considered with and without the tumor in the mesh, producing 6 possible configurations at a given head orientation. To accommodate for potential deviation from the preoperative approximation of the head orientation, 60 probable head orientations were considered, covering ± 20º from the preoperative estimation. Thus, 360 sets of boundary conditions were simulated for gravity-induced shift and similarly 360 sets were modeled for mannitol-induced shift, totaling 720 potential surgical presentations. Lastly, 3 different vascular-based solutions were simulated for swelling-induced shift; to adjust for potential deviation from preoperative approximation of the craniotomy size, 3 different craniotomy sizes (75%, 100% and 125% of the size of the planned craniotomy) were considered, resulting in 9 additional sets of boundary conditions. Moreover, in swelling-induced shift, the craniotomy region was also designated as stress free. The material properties used in describing the boundary conditions may be found in Sun et al. [1]. In summary, a total of 729 unique boundary conditions were generated that represent an exhaustive distribution of potential intraoperative brain shift.

For each boundary condition set, a full volumetric deformation solution was estimated by solving the partial differential equations associated with a biphasic biomechanical model, which is based on Biot's theory of soil consolidation and has been extensively documented in our previous works [1, 23-25]. The resolution of the partial differential equations is done through the Galerkin Method of Weighted Residuals expressed on linear three dimensional basis functions associated with tetrahedral finite elements [26]. Temporal integration is handled by a fully implicit time stepping scheme [26]. The matrix storage and solution libraries were provided by the Portable, Extensible Toolkit for Scientific Computation (PETSc) [27]. The output of this stage is the generation of the deformation atlas containing 729 potential intraoperative brain deformation solutions.

2.4 Deformation Correction

Patient iMR imaging data were rigidly registered to the preoperative imaging data via normalized mutual information. Homologous cortical surface points were selected to provide measurements of surface deformation using 3D Slicer and Analyze 9.0 (AnalyzeDirect, Overland Park, KS) [28]. A pair of such homologous surface points is illustrated in Figure 2, where Figure 2(I) shows a surface feature point on the preoperative MR scan, and Figure 2(II) demonstrates the corresponding surface point selected on the registered intraoperative image.

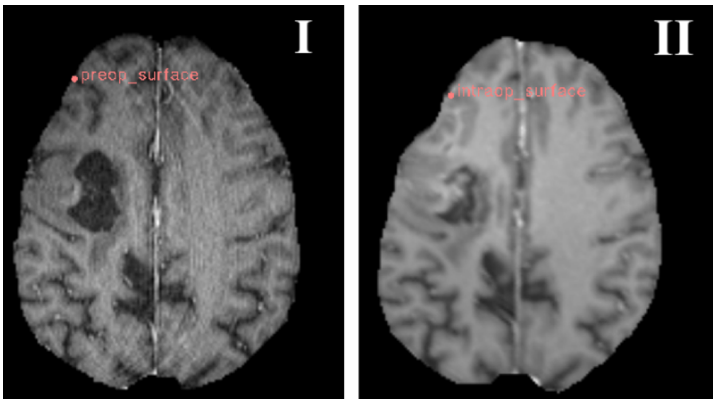

Figure 2. Homologous surface point selection example: (I) a surface point on the preoperative MR image; (II) the corresponding surface point selected on the registered intraoperative MR image.

The surface points were selected near the planned craniotomy, as the exposed cortical surface would be the only source of intraoperative surface information available during a surgery. Once homologous surface points were established, the surface displacement between the preoperative and intraoperative states was computed. This surface deformation was then used to drive the inverse problem, whose objective is to minimize the least squared errors between the measured surface deformation and the predicted deformation that is a combinatory fit drawn from the deformation atlas, or in equation form:

$$\min \|Mw-u\|^2 \ \exists \ w_i \geq 0 \text{ and } \sum_{i=1}^{m} w_i \leq 1 \qquad (1)$$

where M is the subsampled deformation atlas obtained in **Section 2.3** (specifically, M consists of solutions across the atlas but only at the nodes where corresponding measurements are made), u is the surface deformation measured by the selection of homologous surface points above, and w is the weighted coefficients. The additional constraints placed on w in Equation (1) prevents extrapolation and ensures reasonable model prediction of deformation [1]. Once the optimal combination was determined, the full volumetric displacement prediction was used to update the preoperative MR image. A computer with Intel Core i7-4790 CPU @ 3.60GHz with 8 GB of RAM was used to complete the deformation correction process for the two cases investigated.

2.5 Model Performance Assessment—Validation

To evaluate the model's ability to recover intraoperative brain shift, subsurface targets near the tumor region, which are of significant interest to the surgeons, were examined. Similar to **Section 2.4**, homologous subsurface points were selected using 3D Slicer and Analyze 9.0 (AnalyzeDirect, Overland Park, KS), shown in Figure 3, where Figure 3(I) shows a

subsurface landmark on the preoperative image, and Figure 3(II) illustrates the corresponding feature on the intraoperative image [28].

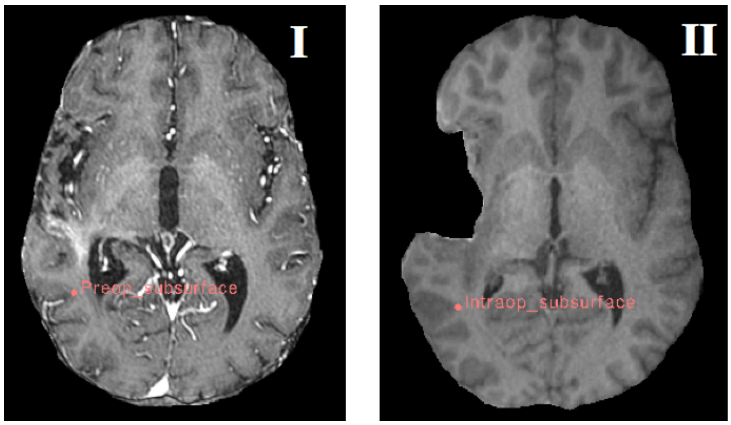

Figure 3. Homologous subsurface point selection example: (I) a subsurface landmark on the preoperative MR image; (II) the corresponding subsurface feature selected on the registered intraoperative MR image.

The selections of homologous subsurface points provide a measurement of subsurface deformation near the tumor region. Additionally, using the volumetric deformation solution obtained in **Section 2.4**, the selected subsurface targets on the preoperative image were mapped onto the model updated image. The transformed points were used to compute the magnitude and direction of the predicted shift. Then the model predicted shift was compared to the measured shift to quantify the accuracy of model correction. In equations:

$$\vec{d}_{actual} = \left(x_i - x_p,\ y_i - y_p,\ z_i - z_p\right) \tag{2}$$

$$\left\|\vec{d}_{actual}\right\| = \sqrt{\left(x_i - x_p\right)^2 + \left(y_i - y_p\right)^2 + \left(z_i - z_p\right)^2} \tag{3}$$

$$\vec{d}_{predicted} = \left(x_m - x_p,\ y_m - y_p,\ z_m - z_p\right) \tag{4}$$

$$\left\|\vec{d}_{predicted}\right\| = \sqrt{\left(x_m - x_p\right)^2 + \left(y_m - y_p\right)^2 + \left(z_m - z_p\right)^2} \tag{5}$$

where d is displacement, subscript i indicates intraoperative space, p presents preoperative space, and m represents the model space after the preoperative image is updated. The residual error of the deformation correction, e, is computed by comparing the results from Equations (2) – (5), and is defined as:

$$\vec{e} = \vec{d}_{predicted} - \vec{d}_{actual} = \left(x_m - x_i,\ y_m - y_i,\ z_m - z_i\right) \tag{6}$$

$$\left\|\vec{e}\right\| = \sqrt{\left(x_m - x_i\right)^2 + \left(y_m - y_i\right)^2 + \left(z_m - z_i\right)^2} \tag{7}$$

The overall percent correction, which reflects the accuracy of the brain shift compensation strategy, is defined as:

$$\text{Percent correction} = 1 - \frac{\left\|\vec{e}\right\|}{\left\|\vec{d}_{actual}\right\|} \tag{8}$$

3. RESULTS

Two patients were analyzed in this preliminary validation study. A total of 48 subsurface landmarks were selected in two cases for validation, and the direction and magnitude of the subsurface shift were obtained by homologous subsurface point selections described in **Section 2.5**. The subsurface shift is stratified into 3 subgroups—low shift defined as below 3 mm, moderate shift between 3 and 6 mm, and high shift above 6 mm. This stratification scheme is similar to the work of Bucholz et al. and is slightly modified to ensure relatively similar sample sizes in the subgroups [29]. Here we consider the model performance in moderate and high shift groups; the exclusion of low shift will be discussed in **Section 4**. Of the 48 subsurface targets selected, 39 resulted in subsurface deformations exceeding 3 mm—25 targets in the moderate shift group and 14 in the high shift group. Overall, average subsurface shift above 3 mm (moderate and high shift) across two cases is 5.5 ± 1.5 mm, and details of the subsurface shift in each case as well as in each subgroup are shown in Table 1.

Table 1. Subsurface shift in two cases analyzed, stratified into 3 subgroups: moderate shift (3 -6 mm), high shift (above 6 mm) and all shifts above 3 mm. The number of points in a particular subgroup is shown in parentheses.

Patient ID	Moderate Shift 3 - 6 mm (mm)	High Shift > 6 mm (mm)	Above 3 mm (mm)
1	4.6 +/- 0.5 (10)	7.7 +/- 1.2 (3)	5.3 +/- 1.5 (13)
2	4.6 +/- 1.0 (15)	6.9 +/- 1.0 (11)	5.6 +/- 1.5 (26)
Combine	4.6 +/- 0.8 (25)	7.1 +/- 1.1 (14)	5.5 +/- 1.5 (39)

Figure 4 illustrates the result of the deformation correction described in **Section 2.4** on one of the patient-specific brain meshes.

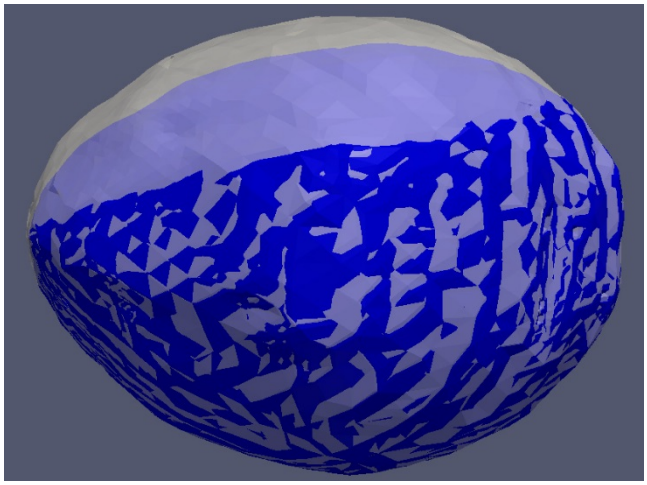

Figure 4. A deformed brain mesh. White semi-transparent mesh is generated from patient preoperative MR image, and the blue mesh is deformed based on the optimal solution of the inverse problem drawn from the deformation atlas.

To evaluate the performance of our brain shift correction algorithm, two quantitative measurements are assessed for subsurface targets: the residual error after the correction in Equation (7) and percent correction described in Equation (8). Overall, the residual error across two cases for moderate and high shift is 2.2 ± 1.2 mm; specifically, the residual error for moderate shift (3 – 6 mm) is 2.3 ± 1.4 mm, and the residual error for high shift (above 6 mm) is 2.2 ± 1.0 mm. Details of the residual error, compare to the measured subsurface deformation, can be found in Table 2.

Table 2. Residual error, described in Equation (7), in two cases analyzed, stratified into 3 subgroups: moderate shift (3 -6 mm), high shift (above 6 mm) and all shifts above 3 mm. The number of points in a particular subgroup is shown in parentheses.

	Moderate Shift (3 – 6 mm)		High Shift (> 6 mm)		Above 3 mm	
Patient ID	**Average Shift (mm)**	**Residual Error (mm)**	**Average Shift (mm)**	**Residual Error (mm)**	**Average Shift (mm)**	**Residual Error (mm)**
1	4.6	1.9 +/- 1.1 (10)	7.7	2.6 +/- 1.4 (3)	5.3	2.1 +/- 1.2 (13)
2	4.6	2.5 +/- 1.5 (15)	6.9	2.1 +/- 1.0 (11)	5.6	2.3 +/- 1.3 (26)
Combine	4.6	2.3 +/- 1.4 (25)	7.1	2.2 +/- 1.0 (14)	5.5	2.2 +/- 1.2 (39)

The percent correction relates residual error to the measured subsurface deformation, and is the second measurement used to gauge the model performance in recovering intraoperative brain shift. For two cases analyzed, the overall percent correction, described in Equation (8), is 59.0% ± 27.7% for moderate and high shift. Specifically, the percent correction for moderate shift (between 3 and 6 mm) is 50.8% ± 31.3% and is 68.5% ± 13.0% for high shift (above 6 mm). The model performance in compensating brain shift across two cases is illustrated in Figure 5.

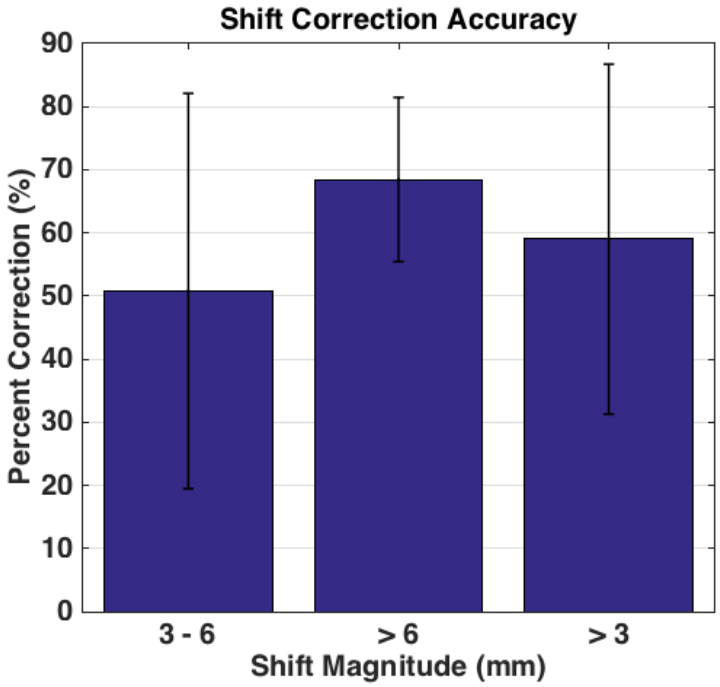

Figure 5. Assessment of shift correction accuracy in two cases. Evaluations, in terms of percent correction expressed in Equation (8), are performed in subgroups of moderate shift, high shift, and all shifts above 3 mm.

The detailed breakdown of model performance, evaluated by percent correction, which is defined in Equation (8), in each case is shown in Table 3.

Table 3. Percent correction, described in Equation (8), in two cases analyzed, stratified into 3 subgroups: moderate shift (3 - 6 mm), high shift (above 6 mm) and all shifts above 3 mm. The number of points in a particular subgroup is shown in parentheses.

Patient ID	Moderate Shift (3 - 6 mm)	High Shift (> 6 mm)	Above 3 mm
1	58.6 +/- 29.1 (10)	66.7 +/- 11.9 (3)	61.3 +/- 26.1 (13)
2	45.5 +/- 32.8 (15)	69.0 +/- 13.8 (11)	57.9 +/- 28.9 (26)
Combine	50.8 +/- 31.3 (25)	68.5 +/- 13.0 (14)	59.0 +/- 27.7 (39)

A paired Student's t-test of the measured subsurface deformation prior to model correction and the residual error after model correction yields a p-value less than 0.001, indicating the differences resulting from the model correction are statistically significant.

4. DISCUSSION

The results of this preliminary validation indicate that the developed deformation atlas based modeling approach to compensate for intraoperative brain shift has the potential to become a complementary technology to iMR in addressing brain shift in neurosurgery. When considering moderate and high shift in two patient cases, the brain shift correction algorithm is able to reduce subsurface deformation from 5.5 mm to 2.2 mm, representing an approximately 59% brain shift recovery. The model performs slightly better in the high shift range, as the average percent correction is greater yet the standard deviation is smaller for high shift targets. Although promising, our experience with these two patients suggests a need for improvements in both our brain shift correction algorithm and our validation study design.

There are several aspects of the validation study design that can be improved. Firstly, the manual designation of homologous points can introduce subjective human errors to the validation results, particularly in finding corresponding features on the intraoperative image volume. For surface homologous point selection, this uncertainty in selecting the corresponding point on the intraoperative scan directly impacts the model prediction, as the surface deformation is the driving force of the inverse approach depicted in **Section 2.4**. For subsurface homologous point selection, the aforementioned uncertainty can similarly impact the validation outcome, as percent correction calculation in Equation (8) depends on the measured subsurface deformation. Going further, in the two patient cases analyzed herein, the voxel spacing of the preoperative MR image volume was $0.4688 \times 0.4688 \times 1.4$ mm for Patient 1, and $0.9766 \times 0.9766 \times 1$ mm for Patient 2. At the very least, partial volume effects in the selection of features would lead to error in corresponding landmark identification (surface and subsurface), and based on the voxel size could easily contribute error on the order of 1 mm, which leaves low shift targets particularly vulnerable. For future validation, it is necessary to carry out a study to investigate the uncertainty in selecting homologous points on intraoperative images and thus gauge the window of potential error introduced by the manual point designation process.

To alleviate the concerns of human errors in designating homologous surface points, future validation studies should also employ more active and real-time monitoring of intraoperative surface deformation during surgery, such as the deployment of laser range scanner (LRS), stereovision, or optical tracking during surgery. LRS, stereovision, or optical tracking can provide a more continuous and accurate assessment of surface deformation. The utilization of LRS and stereovision to measure cortical surface deformation has been an active research project in our laboratory and will be a natural incorporation in our future validation effort [30-33].

Moreover, although we have taken precaution in ensuring the quality of rigid registration of the intraoperative MR image volume to the preoperative space—the preoperative image volume and the registered intraoperative image volume were fused and compared in Analyze 9.0 (AnalyzeDirect, Overland Park, KS), and the alignment of the structures that typically experience little deformation (e.g. orbits and brain stem) was examined—we should note that small errors in the

initial registration can have impacts on the surface and subsurface deformation measurements. A registration sensitivity study needs to be carried out to fully understand the propagation of registration uncertainty toward the model accuracy in compensating for intraoperative brains shift.

Lastly, as a preliminary step toward a more comprehensive validation study, the sample size of this study is limited and a greater sample size—both in the number of patients and the number of subsurface landmarks examined—will provide further confidence in our model-based approach. Similarly, additional data will allow for the further refinement of correction algorithms as well as for determining other aspects that influence shift, e.g. the need for heterogeneity and anisotropy in normal and cancerous brain tissue.

With the errors and limitations expressed above in mind, we observe that the model performance experienced significant variability and inconsistency in the low shift range (less than 3 mm). Without fully assessing the aforementioned errors, the conclusion drawn regarding the low shift correction ability of our model is unconvincing. However, we should note that this should not be interpreted as that our model-based approach being incapable of recovering low shift deformation but rather as a likely failure of obtaining high fidelity measurements to drive the correction approach. A future validation with more salient subsurface targets, and with a better understanding of the impact of the aforementioned errors on the model solution, can better address our model's performance in the low shift range.

5. CONCLUSION

A preliminary validation study of two patients is conducted to examine a deformation atlas based modeling approach to address brain shift in neurosurgery with the current clinical standard, iMR. The results of this study are promising: the developed brain shift correction strategy, based on a biomechanical biphasic model, reduces the subsurface brain shift from 5.5 mm to 2.2 mm, which translates to an approximately 59% brain shift recovery when considering moderate and high shift above 3 mm. The preliminary validation results demonstrate the viability of using a model-based approach to compensate for intraoperative brain shift without significantly disrupting the existing clinical workflow. Future work will involve a study of larger sample size, improvements in validation study design, such as employing active and real-time monitoring of intraoperative surface deformation, and investigate the impact of various errors on the model solution, as well as refinement on the existing correction algorithm.

ACKNOWLEDGEMENT

The rigid and non-rigid registration software was provided by Dr. Benoit Dawant. This work is supported by the National Institutes of Health, the National Institute for Neurological Disorders and Stroke, R01NS049251.

REFERENCE

[1] K. Sun, T. S. Pheiffer, A. L. Simpson, J. A. Weis, R. C. Thompson, and M. I. Miga, "Near Real-Time Computer Assisted Surgery for Brain Shift Correction Using Biomechanical Models," IEEE J Transl Eng Health Med, 2, (2014).

[2] I. Reinertsen, F. Lindseth, C. Askeland, D. H. Iversen, and G. Unsgard, "Intra-operative correction of brain-shift," Acta Neurochir (Wien), 156(7), 1301-10 (2014).

[3] I. J. Gerard, M. Kersten-Oertel, K. Petrecca, D. Sirhan, J. A. Hall, and D. L. Collins, "Brain shift in neuronavigation of brain tumors: A review," Medical Image Analysis, 35, 403-420 (2017).

[4] C. Nimsky, O. Ganslandt, S. Cerny, P. Hastreiter, G. Greiner, and R. Fahlbusch, "Quantification of, visualization of, and compensation for brain shift using intraoperative magnetic resonance imaging," Neurosurgery, 47(5), 1070-1079 (2000).

[5] C. Delorenzo, X. Papademetris, L. H. Staib, K. P. Vives, D. D. Spencer, and J. S. Duncan, "Image-guided intraoperative cortical deformation recovery using game theory: application to neocortical epilepsy surgery," IEEE Trans Med Imaging, 29(2), 322-38 (2010).

[6] J. M. K. Mislow, A. J. Golby, and P. M. Black, "Origins of Intraoperative MRI," Neurosurgery Clinics of North America, 20(2), 137-146 (2009).
[7] C. Nimsky, O. Ganslandt, B. von Keller, J. Romstock, and R. Fahlbusch, "Intraoperative high-field-strength MR imaging: Implementation and experience in 200 patients," Radiology, 233(1), 67-78 (2004).
[8] C. Schulz, S. Waldeck, and U. M. Mauer, "Intraoperative Image Guidance in Neurosurgery: Development, Current Indications, and Future Trends," Radiology Research and Practice, 2012, 197364 (2012).
[9] M. I. Miga, "Computational Modeling for Enhancing Soft Tissue Image Guided Surgery: An Application in Neurosurgery," Annals of Biomedical Engineering, 44(1), 128-138 (2016).
[10] I. Reinertsen, M. Descoteaux, S. Drouin, K. Siddiqi, and D. L. Collins, "Vessel driven correction of brain shift," Medical Image Computing and Computer-Assisted Intervention - Miccai 2004, Pt 2, Proceedings, 3217, 208-216 (2004).
[11] C. DeLorenzo, X. Papademetris, L. H. Staib, K. P. Vives, D. D. Spencer, and J. S. Duncan, "Volumetric intraoperative brain deformation compensation: model development and phantom validation," IEEE Trans Med Imaging, 31(8), 1607-19 (2012).
[12] P. Dumpuri, R. C. Thompson, A. Cao, S. Ding, I. Garg, B. M. Dawant, and M. I. Miga, "A fast and efficient method to compensate for brain shift for tumor resection therapies measured between preoperative and postoperative tomograms," IEEE Trans Biomed Eng, 57(6), 1285-96 (2010).
[13] A. L. Simpson, K. Sun, T. S. Pheiffer, D. C. Rucker, A. K. Sills, R. C. Thompson, and M. I. Miga, "Evaluation of Conoscopic Holography for Estimating Tumor Resection Cavities in Model-Based Image-Guided Neurosurgery," Ieee Transactions on Biomedical Engineering, 61(6), 1833-1843 (2014).
[14] O. Skrinjar, A. Nabavi, and J. Duncan, "Model-driven brain shift compensation," Medical Image Analysis, 6(4), 361-373 (2002).
[15] C. Zhang, M. Wang, and Z. Song, "A brain-deformation framework based on a linear elastic model and evaluation using clinical data," IEEE Trans Biomed Eng, 58(1), 191-9 (2011).
[16] G. R. Joldes, A. Wittek, M. Couton, S. K. Warfield, and K. Miller, [Real-Time Prediction of Brain Shift Using Nonlinear Finite Element Algorithms] Springer Berlin Heidelberg, Berlin, Heidelberg(2009).
[17] L. M. Vigneron, R. C. Boman, J.-P. Ponthot, P. A. Robe, S. K. Warfield, and J. G. Verly, "Enhanced FEM-based modeling of brain shift deformation in Image-Guided Neurosurgery," Journal of Computational and Applied Mathematics, 234(7), 2046-2053 (2010).
[18] P. A. Yushkevich, J. Piven, H. C. Hazlett, R. G. Smith, S. Ho, J. C. Gee, and G. Gerig, "User-guided 3D active contour segmentation of anatomical structures: Significantly improved efficiency and reliability," Neuroimage, 31(3), 1116-1128 (2006).
[19] G. K. Rohde, A. Aldroubi, and B. M. Dawant, "The adaptive bases algorithm for intensity-based nonrigid image registration," IEEE Trans Med Imaging, 22(11), 1470-9 (2003).
[20] J. Ahrens, B. Geveci, and C. Law, [ParaView: An End-User Tool for Large Data Visualization Handbook] Elsevier, (2005).
[21] I. Chen, R. E. Ong, A. L. Simpson, K. Sun, R. C. Thompson, and M. I. Miga, "Integrating Retraction Modeling Into an Atlas-Based Framework for Brain Shift Prediction," IEEE Trans Biomed Eng, 60(12), 3494-504 (2013).
[22] I. Chen, A. M. Coffey, S. Ding, P. Dumpuri, B. M. Dawant, R. C. Thompson, and M. I. Miga, "Intraoperative brain shift compensation: accounting for dural septa," IEEE Trans Biomed Eng, 58(3), 499-508 (2011).
[23] M. I. Miga, K. D. Paulsen, J. M. Lemery, S. D. Eisner, A. Hartov, F. E. Kennedy, and D. W. Roberts, "Model-updated image guidance: Initial clinical experiences with gravity-induced brain deformation," Ieee Transactions on Medical Imaging, 18(10), 866-874 (1999).
[24] K. D. Paulsen, M. I. Miga, F. E. Kennedy, P. J. Hoopes, A. Hartov, and D. W. Roberts, "A computational model for tracking subsurface tissue deformation during stereotactic neurosurgery," Ieee Transactions on Biomedical Engineering, 46(2), 213-225 (1999).
[25] D. W. Roberts, A. Hartov, F. E. Kennedy, M. I. Miga, and K. D. Paulsen, "Intraoperative brain shift and deformation: A quantitative analysis of cortical displacement in 28 cases," Neurosurgery, 43(4), 749-758 (1998).
[26] D. R. Lynch, [Numerical partial differential equations for environmental scientists and engineers : a first practical course] Springer, New York(2005).
[27] S. Balay, W. D. Gropp, L. C. McInnes, and B. F. Smith, [Efficient Management of Parallelism in Object-Oriented Numerical Software Libraries] Birkhäuser Boston, Boston, MA(1997).

[28] A. Fedorov, R. Beichel, J. Kalpathy-Cramer, J. Finet, J. C. Fillion-Robin, S. Pujol, C. Bauer, D. Jennings, F. Fennessy, M. Sonka, J. Buatti, S. Aylward, J. V. Miller, S. Pieper, and R. Kikinis, "3D Slicer as an image computing platform for the Quantitative Imaging Network," Magn Reson Imaging, 30(9), 1323-41 (2012).

[29] R. D. Bucholz, D. D. Yeh, J. Trobaugh, L. L. McDurmont, C. D. Sturm, C. Baumann, J. M. Henderson, A. Levy, and P. Kessman, "The correction of stereotactic inaccuracy caused by brain shift using an intraoperative ultrasound device," Cvrmed-Mrcas'97: First Joint Conference - Computer Vision, Virtual Reality and Robotics in Medicine and Medical Robotics and Computer-Assisted Surgery, 1205, 459-466 (1997).

[30] A. N. Kumar, M. I. Miga, T. S. Pheiffer, L. B. Chambless, R. C. Thompson, and B. M. Dawant, "Persistent and automatic intraoperative 3D digitization of surfaces under dynamic magnifications of an operating microscope," Med Image Anal, 19(1), 30-45 (2015).

[31] A. N. Kumar, T. S. Pheiffer, A. L. Simpson, R. C. Thompson, M. I. Miga, and B. Dawant, "Phantom-based comparison of the accuracy of point clouds extracted from stereo cameras and laser range scanner."

[32] T. S. Pheiffer, A. L. Simpson, B. Lennon, R. C. Thompson, and M. I. Miga, "Design and evaluation of an optically-tracked single-CCD laser range scanner," Medical Physics, 39(2), 636-642 (2012).

[33] T. K. Sinha, M. I. Miga, D. M. Cash, and R. J. Weil, "Intraoperative cortical surface characterization using laser range scanning: preliminary results," Neurosurgery, 59(4 Suppl 2), ONS368-76; discussion ONS376-7 (2006).